Wavelength dependence of the light scattered from a dielectric film deposited on a metal substrate

Ingve Simonsen[a,c], Tamara A. Leskova[b], Alexei A. Maradudin[c],
and Ola Hunderi[a]

[a]Department of Physics, The Norwegian University of Science and Technology,
N-7491 Trondheim, Norway

[b] Institute of Spectroscopy, Russian Academy of Sciences,
Troitsk 142092, Russia

[c]Department of Physics and Astronomy
and Institute for Surface and Interface Science
University of California, Irvine, CA 92697, U.S.A.

ABSTRACT

We consider a scattering system consisting of a dielectric film deposited on a semi-infinite metal, and focus on the wavelength dependence of the total integrated scattering and angle resolved scattering from such a system. In particular we study theoretically by a large scale rigorous numerical simulation approach the reflectivity, $\mathcal{R}(\lambda)$, as well as the total scattered energy, $\mathcal{U}(\lambda)$, of such systems as functions of the wavelength of the incident light. The scattering system consists of vacuum in the region $x_3 > d_1 + \zeta_1(x_1)$, a dielectric film in the region, $d_2 + \zeta_2(x_1) < x_3 < d_1 + \zeta_1(x_1)$, and a metal in the region $x_3 < d_2 + \zeta_2(x_1)$. This system is illuminated from the vacuum side by p-polarized light whose wavelength is allowed to vary from 0.2μm to 1.2μm. The film is assumed to have a dielectric function that is insensitive to the wavelength of the incident light. In obtaining the numerical results reported here the metal substrate is taken to be silver. The dielectric function of silver for a given wavelength is obtained by interpolation from experimental values. The surface profile functions, $\zeta_{1,2}(x_1)$, are assumed to be either zero or single-valued functions of x_1 that are differentiable as many times as is necessary, and to constitute zero-mean, stationary Gaussian random processes. Their surface height auto-correlation function is characterized by a Gaussian power spectrum. We study and discuss the wavelength dependence of $\mathcal{R}(\lambda)$ and $\mathcal{U}(\lambda)$ for several scattering systems obtained by turning on and off the surface profile functions $\zeta_{1,2}(x_1)$ and/or the correlation between these two surface profile functions.

Keywords: reflectivity, dielectric film, surface roughness, Fabry-Perot interference modes, pseudo-Brewster effect

1. Introduction

The use of light scattering, both total integrated scattering and angle resolved scattering, to measure surface roughness has a long history in both physics and technology.[1-7] Not only has the method been the subject of a large number of theoretical investigations, but light scattering systems have also been used in practical applications to access the surface quality of both optical components and mechanical parts.

The purpose of the present work is to study theoretically, by the use of rigorous numerical simulations, the wavelength dependence of the light scattered from one-dimensional, randomly rough, metallic surfaces with a dielectric coating. This problem is of great practical interest. Many metallic surfaces are given a layer that either serves as a protective coating or has specific optical properties, such as an enhanced reflectivity. Both the metal surface and the surface of the dielectric film may be rough, and the roughness of the two surfaces may be either correlated or uncorrelated.

Light scattering calculations have been carried out by the use of a multitude of methods, including geometrical optics, scalar theory, vector theory, numerical simulation approaches, and quantum mechanical perturbative methods.[1-7]

Davis[8] was one of the first to give a theoretical description of light scattering from statistically rough surfaces, and to relate the scattering to the topographical properties of the surface. His theory was, however, restricted to perfectly reflecting surfaces whose root-mean-square (rms) roughness was assumed to be small compared to the wavelength of the incident light. Later Bennett and Porteus[9] generalized Davis' work. Both of these works were based on the scalar Fresnel-Kirchhoff diffraction formulae,[5] and considered only opaque reflecting surfaces.

To include the vector nature of the scattered field requires a different approach. Two dominant methods have been used to study light scattering. The first is a perturbation theory approach. The second is based on the Stratton-Chu equations .[10] The former works well when the rms roughness δ is small compared to the wavelength of the light. In principle perturbation theory may be used to calculate successively higher order solutions, but this becomes progressively more complicated, and high order perturbation theories are not practical.

Most of the works discussed so far have been devoted to scattering from a single surface. However, Elson has studied the scattering of light from surfaces with both single[11] and multiple coatings.[12] His approach was within the framework of perturbation theory and is therefore valid only for small roughness and thin dielectric films.

In this paper we go beyond the small roughness limit. We use a formally exact rigorous numerical simulation approach based on Green's second integral identity in the plane[13] to study the scattering from silver coated by a dielectric film of mean thickness 500nm. Such simulation approaches are frequently used today,[7] but only for a single frequency of the incident light, since such Monte Carlo calculations are computationally expensive. However, in this work we study the wavelength-dependence of the total and specularly scattered energy in the wavelength range 250nm to 1200nm. To our knowledge this is the first such study using a formally exact approach.

2. Scattering Theory

2.1. Scattering system

The one-dimensional film system that will be considered in this paper is depicted in Fig. 1. It consists of a dielectric film deposited on the surface of a semi-infinite metal that will be assumed to be silver. The medium above the film is vacuum. In the most general case both the vacuum-dielectric and the dielectric-metal interfaces are allowed to be randomly rough. In order to guarantee that the film is well-defined we will consider only the case where these two surfaces are non-overlapping. The coordinate system is chosen so that the surfaces are located at $x_3 = d_i + \zeta_i(x_1)$ ($i = 1, 2$) where d_i are real constants with $d_1 \geq 0$ and $d_2 \leq 0$, $i.e$ the origin of the coordinate system is between, or located on one of, the mean (planar) interfaces of the film. Here the index $i = 1$ corresponds to the vacuum-dielectric interface (the upper surface), while $i = 2$ refers to the dielectric-metal interface (the lower surface). Thus, with this convention, vacuum is found in the region $x_3 > d_1 + \zeta_1(x_1)$, the dielectric film in the region $d_2 + \zeta_2(x_1) < x_3 < d_1 + \zeta_1(x_1)$, and the metal occupies the region $x_3 < d_2 + \zeta_2(x_1)$.

The surface profile functions $\zeta_i(x_1)$ are assumed to be single-valued functions of x_1 that are differentiable as many times as needed. Furthermore, they are assumed to constitute zero-mean, stationary, Gaussian random processes defined by

$$\langle \zeta_i(x_1) \rangle = 0, \tag{2.1a}$$
$$\langle \zeta_i(x_1)\zeta_j(x_1') \rangle = \delta^2 W_{ij}(|x_1 - x_1'|). \tag{2.1b}$$

In these expressions $i, j = 1, 2$, δ is the rms height of $\zeta_i(x_1)$ which is assumed to be the same for the two interfaces, and $< \cdot >$ denotes an average over an ensemble of realizations of $\zeta_i(x_1)$. The correlation functions $W_{ij}(|x_1|)$, which obviously are symmetric in the indices i and j, denote in the case $i = j$ just the usual surface height autocorrelation functions, while for $i \neq j$ they are the cross correlation functions between the two interfaces (if we assume that their rms heights are the same). For the cross-correlations between the two surfaces we will assume here that either the two surface profile functions are perfectly correlated ($\zeta_1(x_1) = \zeta_2(x_1)$), in which case $W_{12}(|x_1|) = W_{21}(|x_1|) = W_{11}(|x_1|)$, or that they are completely uncorrelated, $W_{12}(|x_1|) = W_{21}(|x_1|) = 0$.

Furthermore, the correlation functions can be related to the power spectra by

$$g_{ij}(|k|) = \int_{-\infty}^{\infty} dx_1 \, W_{ij}(|x_1|) \, e^{-ikx_1}. \tag{2.2}$$

In the numerical simulation results to be presented below we have assumed Gaussian power spectra exclusively. They have the form

$$g_{11}(|k|) = g_{22}(|k|) = \sqrt{\pi}a \exp\left(-\frac{k^2 a^2}{4}\right), \tag{2.3}$$

where a is the transverse correlation length. Notice that due to Eq. (2.1a) the mean thickness of the dielectric film, with our convention is

$$d = d_1 + |d_2| > 0. \tag{2.4}$$

2.2. Scattering Equations

If the vacuum-dielectric interface $x_3 = d_1 + \zeta_1(x_1)$ is illuminated from the vacuum side by a p-polarized electromagnetic wave of frequency ω, whose plane of incidence is the $x_1 x_3$-plane, the electromagnetic field can fully be described by the nonzero second component of the magnetic field vector. In the region $x_3 > d_1 + \max \zeta_1(x_1)$ it can be written as the sum of an incident beam of finite width and a scattered field:

$$H_2^>(x_1, x_3|\omega) = \int_{-\frac{\omega}{c}}^{\frac{\omega}{c}} \frac{dk}{2\pi} F(k) e^{ikx_1 - i\alpha_0(k,\omega)x_3} + \int_{-\infty}^{\infty} \frac{dq}{2\pi} R(q,\omega) e^{iqx_1 + i\alpha_0(q,\omega)x_3}, \tag{2.5}$$

where $F(k)$ is an envelope function which in principle can be an arbitrary function for which the integral exits. In Eq. (2.5), $R(q,\omega)$ denotes the so-called scattering amplitude, while we have defined

$$\alpha_0(q,\omega) = \begin{cases} \sqrt{\frac{\omega^2}{c^2} - q^2}, & |q| < \omega/c \\ i\sqrt{q^2 - \frac{\omega^2}{c^2}}, & |q| > \omega/c. \end{cases} \tag{2.6}$$

In the present work we will use a Gaussian envelope function defined by[6]

$$F(k) = \sqrt{\pi} \frac{w\omega}{c} \frac{1}{\alpha_0(k,\omega)} \exp\left[-\frac{w^2 \omega^2}{4c^2}\left(\arcsin\frac{ck}{\omega} - \theta_0\right)^2\right], \tag{2.7}$$
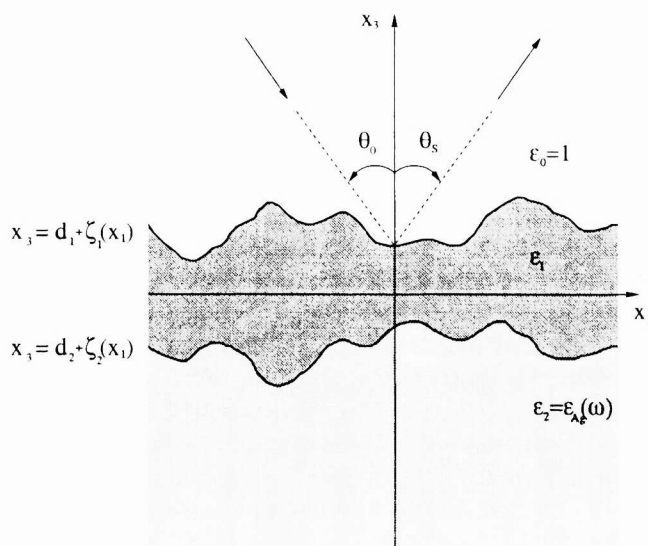

Figure 1. A sketch of the scattering system considered in this work. It consists of vacuum in the region $x_3 > d_1 + \zeta_1(x_1)$, a dielectric film in the region $d_1 + \zeta_1(x_1) < x_3 < d_2 + \zeta_2(x_1)$, and a metal in the region $x_3 < d_2 + \zeta_2(x_1)$. Here $\zeta_i(x_1)$ are random functions with the properties described in the text.

where w denotes the half-width of the incident beam and θ_0 is the angle of incidence.

When the scattering amplitude is known, one can obtain the differential reflection coefficient $\partial R / \partial \theta_s$. It is defined so that $(\partial R / \partial \theta_s) d\theta_s$ is the fraction of the total time-averaged energy flux incident on the surface that is scattered into the angular interval $d\theta_s$ about the scattering angle θ_s in the limit as $d\theta_s \to 0$. The contribution to the mean differential reflection coefficient from the coherent (specular) component of the scattered field is given by[6,7]

$$\left\langle \frac{\partial R}{\partial \theta_s} \right\rangle_{\text{coh}} = \frac{2}{(2\pi)^{\frac{3}{2}}} \frac{\omega}{cw} \cos^2 \theta_s \frac{|\langle R(q,\omega) \rangle|^2}{\frac{1}{2} \left[\text{erf} \left(\frac{w\omega}{\sqrt{2}c} \left(\frac{\pi}{2} + \theta_0 \right) \right) + \text{erf} \left(\frac{w\omega}{\sqrt{2}c} \left(\frac{\pi}{2} - \theta_0 \right) \right) \right]}, \tag{2.8a}$$

where $\text{erf}(\cdot)$ denotes the error function.[18,19] The contribution to the mean differential reflection coefficient from the incoherent (diffuse) component of the scattered field is given by[6,7]

$$\left\langle \frac{\partial R}{\partial \theta_s} \right\rangle_{\text{incoh}} = \frac{2}{(2\pi)^{\frac{3}{2}}} \frac{\omega}{cw} \cos^2 \theta_s \frac{\langle |R(q,\omega)|^2 \rangle - |\langle R(q,\omega) \rangle|^2}{\frac{1}{2} \left[\text{erf} \left(\frac{w\omega}{\sqrt{2}c} \left(\frac{\pi}{2} + \theta_0 \right) \right) + \text{erf} \left(\frac{w\omega}{\sqrt{2}c} \left(\frac{\pi}{2} - \theta_0 \right) \right) \right]}. \tag{2.8b}$$

In Eqs. (2.8), the wave number q is given in terms of the angle of scattering, θ_s by $q = (\omega/c) \sin \theta_s$. This angle is measured clockwise from the x_3-axis as indicated in Fig. 1.

From the knowledge of the mean differential reflection coefficient one may define the reflectance of the surface, $\mathcal{R}(\lambda)$, as

$$\mathcal{R}(\lambda) = \int_{-\frac{\pi}{2}}^{\frac{\pi}{2}} d\theta_s \left\langle \frac{\partial R}{\partial \theta_s} \right\rangle_{\text{coh}}. \tag{2.9}$$

Likewise, the total scattered energy (normalized by the incident energy) is defined by

$$\mathcal{U}(\lambda) = \int_{-\frac{\pi}{2}}^{\frac{\pi}{2}} d\theta_s \left\langle \frac{\partial R}{\partial \theta_s} \right\rangle, \tag{2.10}$$

where $\langle \partial R / \partial \theta_s \rangle$ is the sum of the coherent and incoherent contributions to the mean differential reflection coefficient defined by Eqs. (2.8a) and (2.8b), respectively.

2.3. Excitation of eigenmodes supported by the scattering system

The film system shown in Fig. 1 supports many different types of excitations that might affect the way light is scattered from it. Such excitations includes bulk plasmons, surface plasmons, surface plasmon polaritons, guided waves, Fabry-Perot interference modes, etc. We briefly discuss some of the modes that are relevant for the present work below.

The conduction electrons in the bulk of a metal can execute collective oscillations in a neutralizing background of positive charge, called plasma oscillations, in which their charge density oscillates with a frequency ω_p called the plasma frequency. The plasma frequency is close to the frequency at which the real part of the metal's dielectric function vanishes, and we will denote the (plasma) wavelength at which this happens by $\lambda_p = 2\pi c / \omega_p$. In the numerical simulation results to be presented below we will be considering silver. The dielectric function of silver, $\varepsilon_2(\omega) = \varepsilon_{Ag}(\omega)$, as reported in Palik,[14] is plotted as a function of wavelength in Fig. 2. From this figure it is observed that the plasma wavelength is $\lambda_p \simeq 0.32 \mu m$. This value is also the one observed for silver in the experiments reported in.[15] Notice that in regions where $Re\,\varepsilon_2(\lambda) > 0$ the metal is dielectric–like with a low reflectance, and where $Re\,\varepsilon_2(\lambda) < 0$ it is metal–like and the reflectance is high. The reflectance is therefore expected to make a jump from a low ($\lambda < \lambda_p$) to a high value ($\lambda > \lambda_p$) whenever the wavelength is such that the dielectric function of silver passes through zero.

If both interfaces in Fig. 1 are planar ($\zeta_i(x_1) \equiv 0$) the scattering problem can be solved analytically. The Fresnel coefficient for our scattering system for p-polarization of the incident light reads[16]

$$R_0(k,\omega) = -\frac{\mathcal{D}_-(k,\omega)}{\mathcal{D}_+(k,\omega)}, \tag{2.11a}$$

Guided wave no. modes	λ_{FP} $[\mu m]$
1	0.26
2	0.31
3	0.38
4	0.49
5	0.69
6	1.14

Table 1. The wavelengths of the Fabry-Perot interference modes supported by the scattering system at normal incidence.

where

$$\mathcal{D}_{\pm}(k,\omega) = \left[\varepsilon_0(\omega)\alpha_1(k,\omega) \pm \varepsilon_1(\omega)\alpha_0(k,\omega)\right]\left[\varepsilon_1(\omega)\alpha_2(k,\omega) + \varepsilon_2(\omega)\alpha_1(k,\omega)\right]e^{-i\alpha_1(k,\omega)d}$$
$$+ \left[\varepsilon_0(\omega)\alpha_1(k,\omega) \mp \varepsilon_1(\omega)\alpha_0(k,\omega)\right]\left[\varepsilon_1(\omega)\alpha_2(k,\omega) - \varepsilon_2(\omega)\alpha_1(k,\omega)\right]e^{i\alpha_1(k,\omega)d}. \qquad (2.11b)$$

In Fig. 3 we have plotted the Fresnel reflectivity $|R_0(k,\omega)|^2$ obtained from Eqs. (2.11) as a function of wavelength. The angle of incidence θ_0 is related to the wavenumber k by $k = (\omega/c)\sin\theta_0$, and the angle of incidence assumed in plotting Fig. 3 is $\theta_0 = 0°$. As a function of the wavelength the reflectivity is seen to display a series of minima, whose depths are determined by the absorption in the system. The wavelengths at which they occur are indicated by vertical dotted lines, and are the wavelengths of the so-called Fabry-Perot interference modes of the scattering system[5]. For the range of wavelengths we consider here there are six such modes. Their wavelengths at normal incidence are given in Table 1. The nature of these modes can be understood in the following way.

The solutions of the dispersion relation

$$\mathcal{D}_+(k,\omega) = 0, \qquad (2.12)$$

yield the eigenmodes of the planar system. Their dispersion curves are plotted in Fig. 4. The (ω, k)−plane in Fig. 4 is divided into three regions defined by the straight (dotted) light lines . The right line describes the light propagating
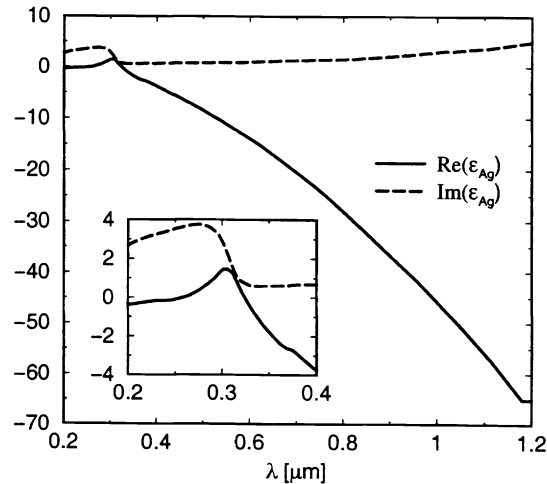

Figure 2. The experimental dielectric function for silver (Ag) as a function of wavelength λ taken from Ref.[14]. The inset shows a detailed view of the wavelength interval from $\lambda = 0.2\mu m$ to $0.4\mu m$.

in the dielectric film along the surface with the dispersion relation

$$k = \sqrt{\varepsilon_1}\frac{\omega}{c}, \tag{2.13}$$

the middle line describes the light propagating along the surface in the vacuum with the dispersion relation

$$k = \sqrt{\varepsilon_0}\frac{\omega}{c}, \tag{2.14}$$

and the left line describes the Brewster mode of the dielectric. The latter has the dispersion relation

$$k = \sqrt{\frac{\varepsilon_0\varepsilon_1}{\varepsilon_0 + \varepsilon_1}}\frac{\omega}{c}. \tag{2.15}$$

For these particular values of ω and k the electromagnetic field does not "feel" the presence of the film deposited on the metal surface. The Fabry–Perot interference modes discussed in the preceding paragraph exist in the radiative region to the left of the vacuum light line. They are the leaky modes of the structure under consideration. The waveguide modes are nonradiative both in the vacuum and the metal, but are wave–like modes in the film. They exist in the region between the vacuum and dielectric light lines. The surface plasmon polaritons exist in the nonradiative region, to the right of the dielectric light line. As $k \to \infty$ the dispersion curve of surface plasmon polaritons saturates at the dispersionless dispersion curve of the surface plasmons that exist at the metal–dielectric interface, whose frequency is determined from the equation

$$\varepsilon_1 + \varepsilon_2(\omega) \quad = \quad 0. \tag{2.16}$$

2.4. Numerical implementation

Before presenting the numerical results, we will make some comments about the numerical implementation used, *i.e.* how we calculated the scattering amplitude $R(q,\omega)$ on which most of the expressions of the preceding subsections rely. There are several ways to calculate this quantity including both perturbative and rigorous numerical simulation approaches. The advantage of a perturbative (approximate) approach is that it needs limited computer resources for its application. However, on the other hand, such a method is restricted to surfaces that can, at the wavelength of the incident light, be considered as weakly rough[4], *i.e.* to surfaces for which

$$2\pi\sqrt{|\varepsilon(\omega)|}\frac{\delta}{\lambda} \quad \ll \quad 1. \tag{2.17}$$
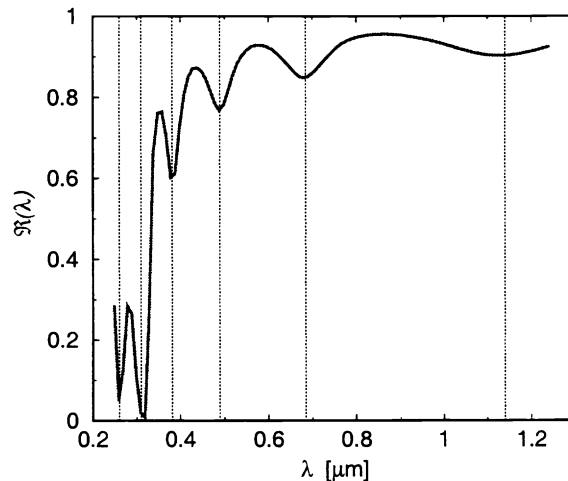

Figure 3. The Fresnel reflectivity at normal incidence for the film system depicted in Fig. 1. The vertical dotted lines indicates the position of the Fabry-Perot interference modes in the dielectric film.
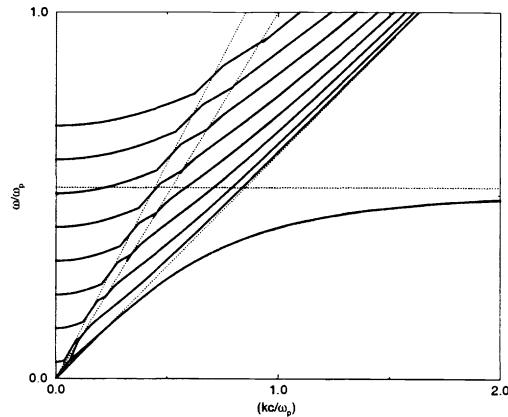
Figure 4. The dispersion curves for the scattering system determined from the relation $\mathcal{D}_+(k,\omega) = 0$. The horizontal dotted line corresponds to the frequency of the surface plasmons determined from $\varepsilon_1 + \varepsilon_2(\omega) = 0$. The three tilted dotted lines correspond from right to left to the dielectric ($\omega = kc/\sqrt{\varepsilon_1}$)) and vacuum ($\omega = kc$) light lines and the Brewster modes ($\omega = kc\sqrt{\varepsilon_0 + \varepsilon_1}/\sqrt{\varepsilon_0\varepsilon_1}$) respectively.

Since we will be interested in the wavelength dependence of $\mathcal{R}(\lambda)$ and $\mathcal{U}(\lambda)$ the above condition is hard to satisfy for all optical wavelengths. In large parts of the roughness-correlation length parameter space this approach does not apply to the surfaces that we will be interested in. Since we are interested in the frequency dependent scattering properties of the system, a change of wavelength might cause a transition from a region where the criterion for the validity of perturbation theory originally was justified to one where it breaks down.

For this reason, we will be using a rigorous numerical simulation approach that is formally exact. However, the disadvantage of this approach is that it requires very significant computational power in order to obtain reliable results. The rigorous approach that we will be using is based on the use of Green's second integral identity in the plane.[13] By taking advantage of this theorem, one can derive a set of four coupled inhomogeneous integral equations for the source functions[7] — the fields and their normal derivatives evaluated on the two interfaces. Discretizing these integral equations leaves us with a matrix system that can be solved by standard techniques[17] for any realization of $\zeta_i(x_1)$. The resulting formulae are given explicitly in Appendix APPENDIX A. We stress that this approach does not assume small roughness and is valid, in principle, for any degree of roughness.

For a given wavelength of the incident light one easily calculates the contributions to the mean differential reflection coefficient from the coherent and incoherent components of the scattered light, Eqs. (2.8), from the solution of the matrix system given by Eqs. (A5). These contributions are then used to calculate the reflectance and total scattered energy, defined by Eqs. (2.9) and (2.10), respectively. For each wavelength of the incident light, λ, at least 500 realizations of the surface profile functions were used in calculating the ensemble average. Furthermore, the calculations were continued by increasing the number of samples in steps of 250 until the reflectance, $\mathcal{R}(\lambda)$, and the total scattered energy, $\mathcal{U}(\lambda)$, had both converged, for that wavelength, to within a relative error of less then 0.5% as compared to the previous logged result for the same quantity. All numerical calculations were performed on an SGI Cray Origin 2000 supercomputer.

3. Results and discussion

Our scattering system allows for two rough surfaces: the vacuum-dielectric and dielectric-metal interfaces. There are thus many different configurations possible that one might consider. We have chosen to study four different configurations defined so that either the (*i*) upper or the (*ii*) lower interface is rough while the other one is planar, or that both interfaces are rough and are perfectly correlated (*iii*) (*i.e.* $\zeta_1(x_1) = \zeta_2(x_1)$), or the two interfaces are (*iv*)

uncorrelated. In all cases the statistical properties of the random functions $\zeta_i(x_1)$ are taken to be the same, when these functions are non-vanishing. They are characterized by an rms height $\delta = 0.025\mu$m, while the surface height autocorrelation function is assumed to be Gaussian with a correlation length $a = 0.1\mu$m. This roughness is enough to make small–amplitude perturbation theory inappropriate for large regions of the wavelength of the incident light considered. The wavelength of the incident light, λ, is allowed to vary in the interval from 0.2μm to 1.2μm. This interval fully includes the wavelengths of visible light. The dielectric film of mean thickness $d = d_1 + |d_2| = 0.5\mu$m has a dielectric function $\varepsilon_1 = 2.6869 + i0.01$ that is assumed to be independent of wavelength over the wavelength range considered. However, the dielectric properties of silver located in the region $x_3 < \zeta_2(x_1)$ are wavelength dependent, and its dielectric function, $\varepsilon_2 = \varepsilon_{Ag}(\lambda)$, is obtained by interpolation from experimentally measured values.[14] The real and imaginary part of this function are plotted as functions of the wavelength in Fig. 2. From the inset in this figure we see that the plasma wavelength of silver is $\lambda_p \simeq 0.32\mu$m ($\varepsilon_{Ag}(\lambda_p) \simeq 0$). Surface plasmons at the film-silver interface should, according to Eq. (2.16), exist for a wavelength $\lambda = \lambda_{sp}$ where $\varepsilon_1 + \varepsilon_{Ag}(\lambda_{sp}) = 0$. From Fig. 2 we find that $\lambda_{sp} \simeq 0.37\mu$m.

In Figs. 5 we show the results of rigorous numerical simulations for the reflectance, $\mathcal{R}(\lambda)$ (lower curves), and the total scattered energy, $\mathcal{U}(\lambda)$ (upper curves), as defined in Subsection 2.2 and obtained by the numerical approach described above. The light was incident normally ($\theta_0 = 0°$) on the dielectric film from the vacuum side.

The first thing we notice from the simulation results of Figs. 5 is that the reflectance $\mathcal{R}(\lambda)$ possess characteristic oscillations. Such oscillations resemble those seen in the Fresnel reflectance (Fig. 3) obtained for the equivalent planar scattering system.[5] For the rough system these oscillations are caused by the same phenomenon that give rise to them in the planar geometry. Hence the local minima of these oscillations are a result of Fabry-Perot interference modes. The reader may check with Table 1 that their positions for the rough scattering systems are practically unaffected by the introduction of roughness. We stress that it is only the wavelength of these modes that survives when roughness is introduced, and not the value of the reflectance itself at a given wavelength. The actual numerical value of the reflectance depends heavily, as can be seen from Figs. 5, on the scattering system considered.

Due to energy conservation a local minimum in $\mathcal{R}(\lambda)$ should (in most cases) be accompanied by a local maximum in $\mathcal{U}(\lambda)$. This can be seen quite clearly from Fig. 5a. Strictly speaking, this statement holds true only if it is absorption due to $Im\,\varepsilon_{Ag}(\omega)$ that is the main source of energy removal from the incident light. In particular, if there exists an eigenmode of the system at the wavelength of the incident light, such a mode may be excited and thus remove energy from the incident light. For such cases it is not clear that there should be a relation between the reflectance and the total scattered energy.

Furthermore, we observe from Figs. 5 that the characteristic jump in $\mathcal{R}(\lambda)$ around the bulk plasma wavelength λ_p found for the planar system (Fig. 3) is washed out when the film-metal interface is made rough (Figs. 5b–d). This is a result of the strongly reflecting rough metal surface causing a substantial fraction of the incident energy to be scattered incoherently away from the specular direction, reducing the specular reflection as a consequence. One can see this in (Figs. 5b–d) as a large difference between the curves corresponding to $\mathcal{R}(\lambda)$ and $\mathcal{U}(\lambda)$. This behavior is not seen for $\mathcal{R}(\lambda)$ if only the vacuum-film interface is rough (Fig. 5a) where, crudely speaking, the reflectance is a downscaled version of the Fresnel reflectance shown in Fig. 3. Moreover, for the total scattered energy $\mathcal{U}(\lambda)$ its value is dramatically increased when the wavelength of the incident light is increased from below to above the plasma wavelength λ_p. This holds true whether the strongly reflecting film-metal surface is rough or not, and is caused by the metal in this wavelength range changing its nature from dielectric–like ($Re\,\varepsilon_2 > 0$) to becoming metal–like ($Re\,\varepsilon_2 < 0$).

By comparing Figs. 3 and 5 and recalling that for a non-rough scattering system the Fresnel reflectivity is equal to the total scattered energy, we observe that introducing roughness at one or both of the interfaces dramatically increases the amount of energy absorbed in the system, or equivalently reduces the total scattered energy $\mathcal{U}(\lambda)$. While the total scattered energy for the planar system case (Fig. 3) for wavelengths $\lambda > \lambda_p$ is about 85–95%, depending on the wavelength, the same quantity is typically reduced to 60% or lower in the same wavelength region when roughness (of the order $\delta \simeq 25$nm) is introduced. That roughness may cause dramatic changes in the total scattered energy is well known and not surprising. However, we find it interesting and somewhat strange at first to observe that the value of $\mathcal{U}(\lambda)$ for $\lambda > \lambda_p$ is consistently lower for the case where *only* the upper interface, *i.e.* the vacuum-film interface, is rough, as compared to the other configurations where the film-metal interface is rough. The explanation for this behavior is as follows. Due to a small dielectric contrast of the scattering interface both the reflection and
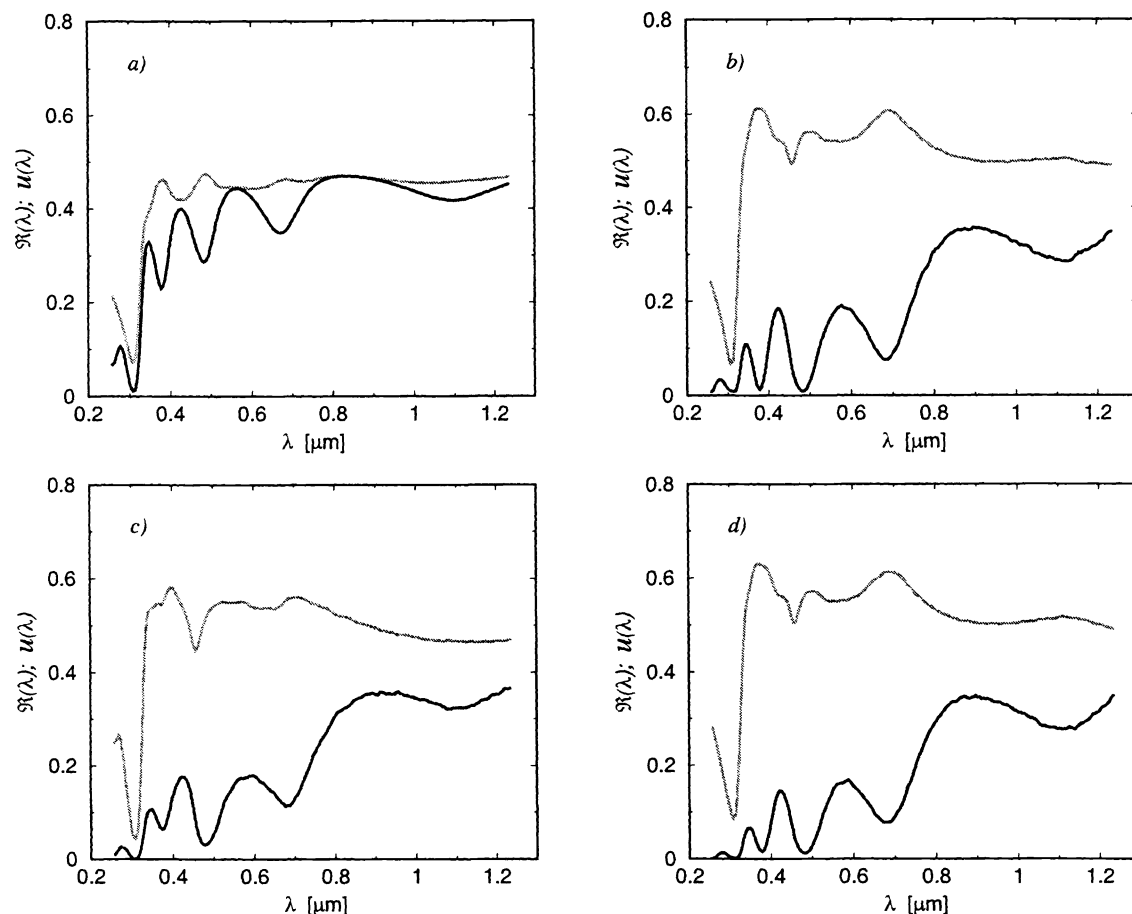
Figure 5. Rigorous numerical Monte Carlo simulation results for the wavelength–dependent reflectance, $\mathcal{R}(\lambda, \theta_0)$, and the total scattered energy, $\mathcal{U}(\lambda, \theta_0)$, as defined in the text, for light of wavelength λ scattered from the scattering system depicted in Fig. 1. The medium $x_3 > d_1 + \zeta_1(x_1)$ was vacuum ($\varepsilon_0 = 1$) and the film ($d_1 + \zeta_1(x_1) < x_3 < d_2 + \zeta_2(x_1)$) of mean thickness of $d = d_1 + |d_2| = 0.500\mu m$ had a wavelength independent dielectric constant $\varepsilon_1 = 2.6869 + i0.01$. The medium in the region $x_3 < d_2 + \zeta_2(x_1)$ was silver, and its dielectric function is plotted in Fig. 2. The surfaces used in the simulations all had a length $L = 25.6\mu m$, and were subdivided into $N = 300$ equally spaced points. A beam of p–polarized waves of wavelength λ with a finite width $g = 6.4\mu m$ was incident on this system at an angle $\theta_0 = 0°$. For each wavelength of the incident light the results for $\mathcal{R}(\lambda, \theta_0)$, and the total scattered energy, $\mathcal{U}(\lambda, \theta_0)$ were averaged over $N_\zeta \geq 500$ surface realizations, and this number was increased (if needed) in steps of 250 until these two quantities had converged to a precision of 0.5% or better. The scattering geometries were such that either the (a) upper or (b) lower surface was rough, or both the upper and lower were rough but in such a way, that they were (c) completely correlated or (d) uncorrelated. The rough surfaces in all cases were assumed to constitute a zero–mean, stationary, Gaussian random process, characterized by an rms-height $\delta = 25$nm and by a Gaussian height autocorrelation function of correlation length $a = 100$nm.

the scattering are weak. However, when the vacuum–film interface is rough the local angle of incidence of light onto the film–metal interface is typically different from zero. Thus, locally the reflection from the planar metal surface becomes weaker, while the absorption increases. Therefore, when the vacuum–film interface is made rough the total scattered energy decreases.

It is also interesting to observe that in the case where only the upper vacuum-film interface is rough the reflectance and total scattered energy are the same for two wavelengths. From the definitions Eqs. (2.9) and (2.10) we realize that

this means that for these wavelengths there is no, or practically no, diffuse scattering even though roughness is present for the scattering system. To understand why this is so, let us consider small–amplitude perturbation theory and, for simplicity, assume a plane incident wave so that the scattering amplitude becomes $R(q|k)$ where $k = (\omega/c)\sin\theta_0$. Since only the vacuum-film interface is rough we find from the criterion (2.17) that we are just at the border of the region in which small–amplitude perturbation theory is valid. Note that if the strongly reflecting film-metal interface is also rough, small–amplitude perturbation theory is not applicable due to the much larger value of $|\varepsilon_{Ag}(\lambda)|$. If we expand the scattering amplitude $R(q|k)$ in powers of the surface profile function, $R(q|k) = \sum_{n=0}^{\infty} R^{(n)}(q|k)/n!$, it can be shown that the lowest order nonspecular term is given by[16]

$$R^{(1)}(q|k) = i\hat{\zeta}_1(q - k)(1 - \varepsilon_1)\frac{\varepsilon_0\varepsilon_1\alpha_0(q)\left[\varepsilon_1\alpha_2(q) + \varepsilon_2\alpha_1(q)\right]}{\mathcal{D}_+(q)}\Sigma(q|k)\frac{\varepsilon_0\varepsilon_1\alpha_0(k)\left[\varepsilon_1\alpha_2(k) + \varepsilon_2\alpha_1(k)\right]}{\mathcal{D}_+(k)} + G(\hat{\zeta}_2),$$

(3.1a)

where $\hat{\zeta}_i(q)$ is the Fourier transform of the surface profile function $\zeta_i(x_1)$, $\mathcal{D}_+(q)$ has been defined earlier in Eq. (2.11b),

$$\Sigma(q|k) = \left\{\frac{\alpha_1(q)\alpha_1(k)}{\varepsilon_1^2}\left[1 + \tilde{r}_{21}(q)\right]\left[1 + \tilde{r}_{21}(k)\right] - \frac{qk}{\varepsilon_1}\left[1 - \tilde{r}_{21}(q)\right]\left[1 - \tilde{r}_{21}(k)\right]\right\},$$

(3.1b)

$G(\hat{\zeta}_2)$ is a *non-vanishing* function for all $\zeta_2(x_1) \neq 0$, and

$$\tilde{r}_{21}(q) = \frac{\varepsilon_1\alpha_2(q) - \varepsilon_2\alpha_1(q)}{\varepsilon_1\alpha_2(q) + \varepsilon_2\alpha_1(q)}\exp\left\{2i\alpha_1(q)d\right\},$$

(3.1c)

is the Fresnel reflection coefficient[5] at the film-metal interface times a phase factor. For the simulation results presented in Fig. 5a the film-metal surface is planar, *i.e.* $\zeta_2 = 0$, with the consequence that $G(\hat{\zeta}_2)$ vanishes. Furthermore, since we are considering normal incidence ($k = 0$) the last term of $\Sigma(q|k)$ vanishes. Now in the limit $|\varepsilon_2| \gg 1$ the reflection coefficient $\tilde{r}_{21}(q)$ becomes

$$\tilde{r}_{21}(q) \simeq -\exp\left\{2i\alpha_1(q)d\right\}, \qquad |\varepsilon_2| \gg 1.$$

(3.2)

If this reflection coefficient is equal to minus one, $\Sigma(q|k)$ as well as the scattering amplitude $R^{(1)}(q|k)$ will vanish. This should happen when $\alpha_1(q)d = n\pi$ for some integer n or for wavelengths

$$\lambda_n \simeq 2\sqrt{\varepsilon_1}\frac{d}{n}, \qquad n = 1, 2, 3, \ldots.$$

(3.3)

This gives for our parameters the wavelengths $\lambda_2 = 0.82\mu\text{m}$, $\lambda_3 = 0.55\mu\text{m}$, $\lambda_4 = 0.41\mu\text{m}$, etc. Since the condition $|\varepsilon_2| \gg 1$ is satisfied best for the longest wavelengths, one should expect, based on small–amplitude perturbation theory, that the diffuse scattering will disappear only for the largest wavelengths. This is indeed supported by the numerical simulations results presented in Fig. 5a, from which it is seen that $\mathcal{R}(\lambda) = \mathcal{U}(\lambda)$ for the wavelength $\lambda \simeq \lambda_2$ to the accuracy that we have in the numerical simulations. Already for $\lambda = \lambda_3$ there seems to be a small fraction of diffuse scattering. This is particularly noticeable for wavelengths λ_n with $n > 3$. For such wavelengths also the assumption made above that $|\varepsilon_2(\lambda)| \gg 1$ is starting to become questionable. The wavelengths that we read off from our numerical simulation result that correspond to λ_2 and λ_3 are respectively $0.82\mu\text{m}$ and $0.56\mu\text{m}$. Notice that the phenomenon described above is unique to normal incidence $\theta_0 = 0°$. For non-normal incidence the second term of $\Sigma(q|k)$ can not be made to vanish at the same time as the first term. Furthermore, from Eq. (3.1a) we notice that when the lower interface is rough, $\zeta_2(x_1) \neq 0$, independent of what the upper interface is, the effect is not present since then $G(\hat{\zeta}_2) \neq 0$ and therefore $R^{(1)}(q|k)$ will not vanish.

Furthermore, $\mathcal{U}(\lambda)$, for all geometries considered, varies only slightly ($\pm 10\%$) for wavelengths $\lambda > \lambda_p$, and its level in this wavelength range seems to be 50–60%. Furthermore, for $\mathcal{R}(\lambda)$ we observe wavelength–dependent oscillations. These are of the same type and origin as those observed in the case of a planar geometry (see Fig. 3).

Another characteristic feature that can be seen in the simulation results presented in Figs. 5 are the distinguished dips that occur at the wavelength $\lambda_d \simeq 0.45\mu\text{m}$. These dips occur only when the film-metal interface is rough and

must therefore be related to a phenomenon that takes place at the film-metal interface. They occur at a wavelength where the reflectance has a minimum at the "quasi-Brewster angle". Since the surface is rough, we have all angles of incidence onto the film-metal interface including quite large angles. The scattering potential does not have any zeros or minima when the film-metal interface is rough. However, the total (integrated) scattered energy, $\mathcal{U}(\lambda)$, as defined by Eq. (2.10), has a minimum, and the wavelength of this minimum is the one at which the quasi-Brewster angle moves into the radiative region of the vacuum. By using small-amplitude perturbation theory, the frequency positions of the dips can be estimated. They can be shown to fall into the frequency region defined by[20]

$$\varepsilon_1^2 + \varepsilon_2(\omega) = 0, \qquad (3.4)$$

which is due to the quasi–Brewster effect at the dielectric–metal interface. The high local slopes of the rough dielectric–metal interface makes it possible to observe the dips. With the dielectric function of silver plotted in Fig. 2, Eq. (3.4) defines a wavelength of the dip consistent with λ_d given above and obtained from the simulations. From the numerical simulation results there seems to be no good evidence of excitations of surface plasmons. This we believe to be related to the fact that in our case the surface plasmon polaritons are strongly damped by the interface roughness.

4. Conclusions

We have studied by a rigorous numerical simulation approach the wavelength dependence of the reflectance, $\mathcal{R}(\lambda)$, and the total scattered energy, $\mathcal{U}(\lambda)$, for light of wavelength $\lambda \simeq 0.2$–$1.2\mu m$ incident normally on a system consisting of a dielectric film ($\varepsilon = 2.6869 + i0.01$) of mean thickness $0.5\mu m$ deposited on the surface of a semi–infinite silver substrate. The medium of incidence located above the dielectric film was vacuum, and for the dielectric function of silver we used experimental values as reported in Palik.[14] It is found, as is well known, that introducing roughness into at least one of the two interfaces reduces the total scattered energy dramatically. However, what is more surprising, we have found that the total scattered energy is reduced the most by making the vacuum-film interface rough while at the same time keeping the film-metal interface planar. We attribute this behavior to the enhancement of the absorption in the metal. It is also shown that the Fabry-Perot interference modes that exist for the geometry considered, and which are easily seen in $\mathcal{R}(\lambda)$, are rather robust and are not much changed by introducing roughness into the scattering system. However, there seems to be no evidence for the excitation of the surface plasmon polariton of the three–layer system, which can be attributed to the strong roughness-induced damping of surface plasmon polaritons. The well–pronounced dip of the total scattered intensity (a peak in the absorptivity) at $\lambda = 0.45\mu m$ we attribute to the maximum of the absorption by the rough metal surface due to the quasi–Brewster effect.

Acknowledgments

APPENDIX A. The integral equations

In this appendix we give the matrix elements for the matrix system used in calculating the scattering amplitude $R(q|k)$ for the film system of Fig. 1. In order to simplify the notation we introduce some index conventions. In order to distinguish the different materials we will use subscript μ, where $\mu = 1$ refers to vacuum, $\mu = 2$ to the film, and $\mu = 3$ to the metal. A surface index σ will also be used, where $\sigma = 1$ refers to the vacuum-dielectric interface, while $\sigma = 2$ denotes the dielectric-metal interface. The index ν is a polarization index taking on values $\nu = p, s$. In our case, it should be put equal to $\nu = p$.

With these conventions the source functions — the fields and their normal derivatives evaluated on the interfaces — become, respectively,

$$\mathcal{F}_\nu^{(\sigma)}(x_1|\omega) = \left. \Phi_\nu^{(\sigma)}(x_1, x_3|\omega) \right|_{x_3 = d_\sigma + \zeta_\sigma(x_1)} \qquad (A.1a)$$

$$\mathcal{N}_\nu^{(\sigma)}(x_1|\omega) = \left. \gamma_\sigma(x) \, \partial_{n_\sigma} \Phi_\nu^{(\sigma)}(x_1, x_3|\omega) \right|_{x_3 = d_\sigma + \zeta_\sigma(x_1)} . \qquad (A.1b)$$

In these equations $\Phi_\nu(x_1, x_3|\omega)$ denotes the fields and is defined as $\Phi_p(x_1, x_3|\omega) = H_2(x_1, x_3|\omega)$ and $\Phi_s(x_1, x_3|\omega) = E_2(x_1, x_3|\omega)$ for p- and s-polarization, respectively. Furthermore, we have defined

$$\gamma_\sigma(x_1) = \sqrt{1 + [\zeta'_\sigma(x)]^2}, \tag{A.2a}$$

$$\partial_{n_\sigma} = \frac{\partial_{x_3} - \zeta'_\sigma(x)\partial_{x_1}}{\gamma_\sigma(x)}, \tag{A.2b}$$

where $\partial_{x_i} = \partial/\partial x_i$. Notice that $\gamma_\sigma(x)\,\partial_{n_\sigma}$ is nothing else but the unnormalized normal derivative.

In terms of the source functions $\mathcal{F}_\nu^{(\sigma)}(x_1|\omega)$ and $\mathcal{N}_\nu^{(\sigma)}(x_1|\omega)$ the scattering amplitude is defined as

$$R_\nu^{(\sigma)}(q,\omega) = \frac{i}{2\alpha_0(q,\omega)} \int_{-\infty}^{\infty} dx_1\, e^{iqx_1 - i\alpha_0(q,\omega)\zeta(x_1)} \left[i\left\{ q\zeta'(x_1) - \alpha_0(q,\omega) \right\} \mathcal{F}_\nu^{(\sigma)}(x_1) - \mathcal{N}_\nu^{(\sigma)}(x_1) \right]. \tag{A.3}$$

If the equidistant discretization

$$\xi_m = -\frac{L_1}{2} + (m + \frac{1}{2})\Delta\xi \qquad m = 1, 2, 3, \ldots, N, \tag{A.4}$$

is introduced, where $\Delta\xi = L/N$, the matrix equations that determine the source functions take the following forms

$$\mathcal{F}_\nu^{(1)}(\xi_m|\omega) = \mathcal{F}_\nu^{inc}(\xi_m|\omega) + \sum_{n=1}^{N} \left[\mathcal{A}_{mn}^{(1;11)} \mathcal{F}_\nu^{(1)}(\xi_n|\omega) - \mathcal{B}_{mn}^{(1;11)} \mathcal{N}_\nu^{(1)}(\xi_n|\omega) \right], \tag{A.5a}$$

$$0 = \sum_{n=1}^{N} \left[\mathcal{A}_{mn}^{(2;11)} \mathcal{F}_\nu^{(1)}(\xi_n|\omega) - \frac{\kappa_\nu^{(2)}(\omega)}{\kappa_\nu^{(1)}(\omega)} \mathcal{B}_{mn}^{(2;11)} \mathcal{N}_\nu^{(1)}(\xi_n|\omega) - \mathcal{A}_{mn}^{(2;12)} \mathcal{F}_\nu^{(2)}(\xi_n|\omega) + \mathcal{B}_{mn}^{(2;12)} \mathcal{N}_\nu^{(2)}(\xi_n|\omega) \right], \tag{A.5b}$$

$$\mathcal{F}_\nu^{(2)}(\xi_m|\omega) = \sum_{n=1}^{N} \left[-\mathcal{A}_{mn}^{(2;21)} \mathcal{F}_\nu^{(1)}(\xi_n|\omega) + \frac{\kappa_\nu^{(2)}(\omega)}{\kappa_\nu^{(1)}(\omega)} \mathcal{B}_{mn}^{(2;21)} \mathcal{N}_\nu^{(1)}(\xi_n|\omega) + \mathcal{A}_{mn}^{(2;22)} \mathcal{F}_\nu^{(2)}(\xi_n|\omega) - \mathcal{B}_{mn}^{(2;22)} \mathcal{N}_\nu^{(2)}(\xi_n|\omega) \right], \tag{A.5c}$$

$$0 = \sum_{n=1}^{N} \left[\mathcal{A}_{mn}^{(3;22)} \mathcal{F}_\nu^{(2)}(\xi_n|\omega) - \frac{\kappa_\nu^{(3)}(\omega)}{\kappa_\nu^{(2)}(\omega)} \mathcal{B}_{mn}^{(3;22)} \mathcal{N}_\nu^{(2)}(\xi_n|\omega) \right], \tag{A.5d}$$

where

$$\kappa_\nu^{(\mu)}(\omega) = \begin{cases} \varepsilon_\mu(\omega) & \nu = p, \\ 1 & \nu = s, \end{cases} \tag{A.6}$$

and the matrix elements are defined as

$$\mathcal{A}_{mn}^{(\mu;\sigma\sigma')} = \begin{cases} \frac{1}{2} + \frac{\Delta\xi}{4\pi} \frac{\zeta''_\sigma(\xi_m)}{1 + [\zeta'_\sigma(\xi_m)]^2} & \sigma = \sigma'; m = n \\ \Delta\xi\, A_{\mu;\sigma\sigma'}(\xi_m|\xi_n) & \text{otherwise}, \end{cases} \tag{A.7}$$

$$\mathcal{B}_{mn}^{(\mu;\sigma\sigma')} = \begin{cases} \frac{i}{4}\Delta\xi\, H_0^{(1)}\left(\sqrt{\varepsilon_\mu(\omega)} \frac{\omega}{c} \frac{\Delta\xi}{2e} \sqrt{1 + [\zeta'_\sigma(\xi_m)]^2} \right) & \sigma = \sigma'; m = n \\ \Delta\xi\, B_{\mu;\sigma\sigma'}(\xi_m|\xi_n) & \text{otherwise}, \end{cases} \tag{A.8}$$

where $A_{\mu;\sigma\sigma'}(x_1|x_1')$ and $B_{\mu;\sigma\sigma'}(x_1|x_1')$ are the kernels of the underlying inhomogeneous integral equations. They are defined as

$$A_{\mu;\sigma\sigma'}(x_1|x_1') = \frac{1}{4\pi} \gamma_\sigma(x_1)\, \partial_{n'_{\sigma'}} G_\mu(x_1, x_3|x_1', x_3') \Big|_{\substack{x_3 = d_\sigma + \zeta_\sigma(x_1) + \eta \\ x_3' = d_{\sigma'} + \zeta_{\sigma'}(x_1')}}$$

$$= -\frac{i}{4}\varepsilon_\mu(\omega)\,\frac{\omega^2}{c^2}\,\frac{H_1^{(1)}\left(\sqrt{\varepsilon_\mu(\omega)}\frac{\omega}{c}\sqrt{(x_1-x_1')^2+\{d_\sigma+\zeta_\sigma(x_1)-d_{\sigma'}-\zeta_{\sigma'}(x_1')+\eta\}^2}\right)}{\sqrt{\varepsilon_\mu(\omega)}\frac{\omega}{c}\sqrt{(x_1-x_1')^2+\{d_\sigma+\zeta_\sigma(x_1)-d_{\sigma'}-\zeta_{\sigma'}(x_1')+\eta\}^2}}$$
$$\times\left[(x_1-x_1')^2\zeta_{\sigma'}'(x_1')-\{d_\sigma+\gamma_\sigma(x_1)-d_{\sigma'}-\gamma_{\sigma'}(x_1')+\eta\}^2\right] \tag{A.9}$$

$$B_{\mu;\sigma\sigma'}(x_1|x_1') = \frac{1}{4\pi}\,G_\mu(x_1,x_3|x_1',x_3')\Bigg|_{\substack{x_3=d_\sigma+\zeta_\sigma(x_1)+\eta \\ x_3'=d_{\sigma'}+\zeta_{\sigma'}(x_1')}}$$
$$= -\frac{i}{4}H_0^{(1)}\left(\sqrt{\varepsilon_\mu(\omega)}\frac{\omega}{c}\sqrt{(x_1-x_1')^2+\{d_\sigma+\zeta_\sigma(x_1)-d_{\sigma'}-\zeta_{\sigma'}(x_1')+\eta\}^2}\right), \tag{A.10}$$

where η is a positive infinitesimal. Furthermore, $G_\mu(x_1,x_3|x_1',x_3')$ denotes the Green's function for the two-dimensional Helmholtz equation,[19] and $H_i^{(1)}(\cdot)$ is the Hankel function of the first kind .[18]

References

1. J. M. Elson, H. E. Bennett, and J. M. Bennett, *Applied Optics and Optical Engineering*, Vol. VII, (Academic Press Inc., 1979).

2. P. Beckmann and A. Spizzichino, *The Scattering of Electromagnetic Waves from Rough Surfaces*, (Artech House, 1963).

3. A. G. Voronovich, *Wave Scattering from Rough Surfaces*, (Springer–Verlag, New York, 1994).

4. J. A. Ogilvy, *Theory of Wave Scattering from Random Rough Surfaces*, (IOP Publishers, Bristol, UK, 1991).

5. M. Born and E. Wolf, *Principles of Optics : Electromagnetic Theory of Propagation, Interference and Diffraction of Light*, 7th (expanded) edition, (Cambridge University Press, Cambridge, 1999).

6. A. A. Maradudin, T. Michel, A. R. McGurn, and E. R. Méndez, Ann. Phys. **203**, 255 (1990).

7. V. Freilikher, E. Kanzieper, and A. A. Maradudin, Phys. Rep. **288**, 127 (1997).

8. H. Davis, Proc. IEEE **101**, 209 (1954).

9. H. E. Bennett and J. O. Porteus, J. Opt. Soc. Am. A **51**, 123 (1961).

10. J. A. Kong, *Electromagnetic Wave Theory*, (John Wiley and Sons, New York, 1990), Section 5.3a.

11. J. M. Elson, J. Opt. Soc. Am. A **66**, 682 (1976).

12. J. M. Elson, J. P. Rahn, and J. M. Bennett, Appl. Opt. **22**, 3207 (1983).

13. A. E. Danese, *Advanced Calculus*, (Allyn and Bacon, Boston, & Sons, 1965), p.123.

14. E. D. Palik, *Handbook of Optical Constants of Solids*, (Academic Press, New York, 1985).

15. F. Abeles, in *Surface Polaritons—Electromagnetic Waves at Surfaces and Interfaces*, ed. V. M. Agranovich and D. L. Mills, (North-Holland Publishing Company, 1982).

16. T. A. Leskova, E. I. Chaikina, G. Navarrete, and G. Martínez-Niconoff, Phys. Rev. B **59**, 11 062 (1999).

17. W. H. Press, S. A. Teukolsky, W. T. Vetterling and B. P. Flannery, *Numerical Recipes*, 2nd edition, (Cambridge University Press, Cambridge, 1992), pp. 281 and 282.

18. M. Abramowitz and I. A. Stegun, *Handbook of Mathematical Functions*, (Dover, New York, 1964).

19. P. M. Morse and H. Feshbach, *Methods of Theoretical Physics*, Part 1 and 2, (McGraw-Hill, New York, 1953).

20. T. A. Leskova, unpublished work (2000).